Adhesive Quality Inspection System Based on Air-Coupled Ultrasonic Waves

Qianpeng Yin,[a] Dewei Gao,[b] Jun Wang,[c] Yingchao Li,[d] Liming Song,[e] Hongyan Zou,[a] and Zheng Wang [f,*]

There has been a lack of in-depth research on plywood quality inspection. There are problems that cannot be detected with current methods due to an insufficiency of inspection methods, low inspection efficiency, and the internal nature of some wood defects. This paper describes the design, software, and experimental verification of a new plywood quality inspection system based on air-coupled ultrasound. An ultrasonic C-scanning platform was designed and constructed. Features selected included a core detection devices, signal excitation module, signal processing module, and motion control module design. The software system design included a host computer interface, C-scanning motion control, MCU excitation signal output, serial communication, ultrasonic C-scanning imaging, as well as interpolation algorithms, *etc.* The validation test during the inspection of plywood shows that the system was able to realize accurate positioning detection of common plywood defects, such as blisters and plywood seams, and determine the location and shape of plywood defects. The above can provide technical support for the online quality inspection of plywood products, which is of high practical significance.

DOI: 10.15376/biores.21.3.7572-7591

Keywords: Plywood; Ultrasonic non-destructive testing; Air coupling; LabVIEW; Signal correlation

Contact information: a: College of Mechanical and Electronic Engineering, Nanjing Forestry University, Huaian, 223231, China; b: People's Government of Qingong Township, Huai'an District, Huai'an City, Nanjing, 210037, China; c: College of Information Science and Technology, Nanjing Forestry University, Lianyungang, 222506, China; d: Jiangsu Yindelong Wood Industry Limited Company, Hangzhou, 311200, China; e: Zhejiang Jindi Holdings Group Co., Ltd., Nanjing, 210037, China; f: College of Materials Science and Engineering, Nanjing Forestry University, Nanjing, 210037, China;
** Corresponding author: wangzheng63258@163.com*

INTRODUCTION

Since the beginning of the 21st century, China's manufacturing industry has experienced unprecedented growth. Concurrently, factors such as population growth, improvements in living standards, and increased consumer purchasing power, have led to a rise in market demand for forest products (Liang *et al.* 2022). China is a leading producer and exporter of plywood, which also accounts for the largest share of both production and consumption of engineered wood products (Wang 2022). In the production of plywood, various quality defects, such as blisters (void spaces caused by entrapped gas between veneer layers), joint separation, and local adhesion failure often occur (Liang *et al.* 2022). Blistering is a defect characterized by raised areas caused by gas trapped within the surface layer of plywood; an adhesion defect refers to the separation phenomenon between the adhesive layers of adjacent veneers; seam separation pertains to the issues arising at the overlaps of plywood surfaces where adhesion is insufficient. Clearly, these defects can noticeably impact the quality of plywood, directly affecting the economic benefits and reputation of manufacturers.

The application of advanced non-destructive testing technologies to assess the overall quality of plywood is of considerable practical significance for manufacturers seeking to optimize structural design and production processes. Currently, many plywood manufacturers primarily depend on traditional visual inspection methods to identify quality defects, such as blistering and seam separation. The reliance on visual inspection methods can introduce subjectivity among inspectors, adversely affecting plywood quality; furthermore, this approach is inefficient and leads to wastage of wood resources. Consequently, manufacturers urgently require advanced, non-destructive, scientific, and cost-effective testing methods, such as modern ultrasonic method and vibration method (Wang *et al.* 2015; Wang *et al.* 2016, 2018; Liu 2019), to effectively and rapidly test and evaluate the quality of plywood products. Among these methods, the ultrasonic method uses the time difference and signal peaks of ultrasonic radiation to determine the quality of wood. Typically, conventional ultrasonic wood inspection requires the application of a coupling agent at the probe interfaces on both sides of the specimen to minimize ultrasonic energy attenuation in air.

However, this method may lead to the penetration of the coupling agent into the wood's interior, potentially contaminating the material and compromising its structure, which can result in inaccuracies in detection outcomes (Livings *et al.* 2016; Li and Zhou 2019). Consequently, this study investigates the application of air-coupled ultrasonic non-destructive testing technology. This technology employs air as the coupling medium. This approach eliminates the need for liquid coupling agents and achieving true non-contact non-destructive testing. The system is capable of detecting quality defects in various types of plywood of differing thicknesses, thereby enhancing quality grading, production efficiency, and economic benefits. With the scanning parameters adopted in this study, a single panel can be scanned in approximately 1 to 2 minutes with computation completed in under 15 seconds, thereby enabling integration with automatic process control. Since air is the coupling medium, the transducer-to-surface distance critically affects signal quality; the optimal total transducer spacing was experimentally determined to be 15 cm, as detailed in the experimental section.

Currently, research on material defects utilizing ultrasonic methods has yielded significant results worldwide (Castaings *et al.* 1998; Bustamante *et al.* 2020). In 1989, Shi was among the first researchers to propose the application of ultrasonic methods for the detection and analysis of defects and defect depths in workpieces. He experimentally demonstrated that the maximum reflection method using ultrasonic transverse waves is a simple, accurate, and rapid technique for detecting surface opening defects (Shi 1989). In 2010, Akseli introduced a non-contact, non-destructive air-coupled ultrasonic technique for assessing the mechanical properties of double-layer tablets (Akseli *et al.* 2010). In 2015, Chennamsetti evaluated the radiation patterns of 100 kHz, 200 kHz, and 500 kHz air-coupled transducers on 1-mm- and 3-mm-thick aluminum plates, employing a fixed transmitter position while moving the receiver transducer along a fixed radius (Chennamsetti *et al.* 2015). A Gaussian fit was derived to accurately characterize the amplitude variations of the A0 modes radiated by the air-coupled probes in an isotropic medium. Also in 2015, In *et al.* employed fully non-contact, air-coupled ultrasonic measurements to detect surface-breaking cracks in concrete, demonstrating that the technique could accurately characterize crack dimensions without any physical contact with the specimen surface (In *et al.* 2015). In 2016, Dongbo Zhang utilized an aluminum plate and other plates as test samples, and used Lamb wave detection on one side of the aluminum plate through the air-coupled plate structure sound transmission model based on the potential function method. Their results indicated that the signal propagation through the half-through-hole defects would generate extreme values, and the aluminum plate half-through-hole defects could be accurately located by using the S0 and A0 modes (Zhang *et al.* 2016). In the same year, Guan Tsuen colleagues designed an air-coupled ultrasonic non-destructive testing system and developed a dedicated signal processing module incorporating multiple pulse compression algorithms, integrating various functional modules for receiving and processing signals (Gui *et al.* 2016). In 2017, Khan employed a three-axis automated non-contact ultrasonic inspection scanner with a C-scanning mode to detect the internal defects and properties of carbon brake disc composites, which confirms that the defects and properties of carbon brake disc composites can be detected when the medium and the air interface is covered by a material that ultrasonic waves cannot propagate, the accuracy of the C-scan images and the detection of internal defects are greatly improved (Khan *et al.* 2017). In 2020, Quattrocchi employed non-contact ultrasonic C-scanning to evaluate the effect of operating parameters on the detection of artificial defects inside GFRP. The results of the study indicated that the ultrasonic beam focusing situation, scanning step size, scanning speed and received signal gain influence the sensitivity of the C-scan image (Quattrocchi *et al.* 2020). Notably, Sanabria *et al.* (2011) demonstrated that air-coupled ultrasound could serve as an accurate and reproducible method for assessing the bonding quality of glued timber, confirming the technique's suitability for evaluating adhesive interfaces in engineered wood products—a finding directly relevant to the plywood quality inspection objectives of the present study (Sanabria *et al.* 2011).

In summary, both domestic and international research on non-destructive testing of plywood quality suffers from a lack of targeted and in-depth studies, limited detection methods, and low detection accuracy. To address this issue, this study involved the development of a plywood quality inspection system based on air-coupled ultrasonic waves, involving the design of both software and hardware systems and the construction of an ultrasonic C-scanning platform. This system facilitates rapid scanning and imaging of plywood, effectively locating defects, and provides support for online quality inspection of plywood.

Design and Construction of the Detection Experiment System

The system primarily comprises an ultrasonic transducer, an excitation module, a reception module, upper computer operation interface, a C-scanning platform, and a power supply, as illustrated in Fig. 1. Notably, the central frequency of the ultrasonic transducer is 200 kHz. The excitation signal is generated by the DAC module of the STM32, while the visual data acquisition and processing platform based on LabVIEW is responsible for the acquisition and processing of ultrasonic signals. The upper computer operation interface facilitates the parameter setting and transmission for stepper motor operations, enables the retrieval of imaging data, and performs imaging tasks. Additionally, the C-scanning platform allows for the control of the C-scan motion trajectory and the operation of X and Y-axis stepper motors.

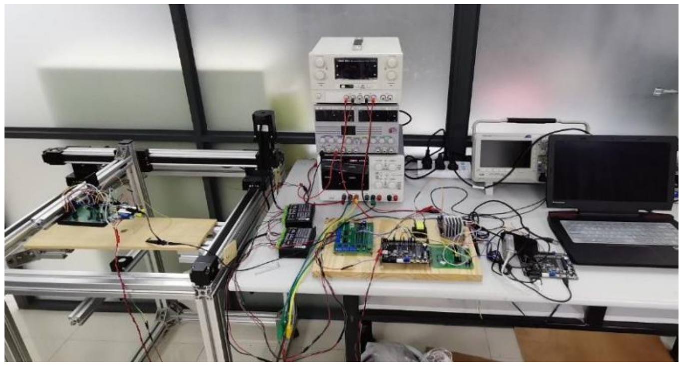

Fig. 1. Physical diagram of the detection system

Air-coupled Ultrasonic Detection Imaging Principle

Compared to other waveforms, ultrasound offers advantages such as shorter wavelength, improved directivity, and greater penetration capability. As a novel detection technology, it holds significant promise in the field of non-destructive testing of materials such as wood and steel (Song *et al.* 2020). During propagation, when ultrasound encounters a change in medium, various phenomena occur, such as energy attenuation, penetration, reflection, and changes in propagation speed. These phenomena alter the parameters related to the ultrasonic signal, enabling the detection of internal material defects through the study and analysis of these parameter changes, as well as achieving defect localization (Li *et al.* 2020). Figure 2 illustrates the structure of the air-coupled ultrasonic C-scan imaging system, where a matched pair of ultrasonic transducers is fixed to the scanning bracket. Point-by-point detection is performed in the designated area, as indicated in Fig. 2, ultimately constructing the image based on the amplitude of the ultrasonic signal or the propagation time during detection. The imaging principle primarily involves amplitude imaging and time-delay imaging. Amplitude imaging correlates the waveform at both the intact and defective positions of the plywood, while the time-lapse imaging method is based on the correlation of the time difference between passing through the intact and defective positions of the plywood.

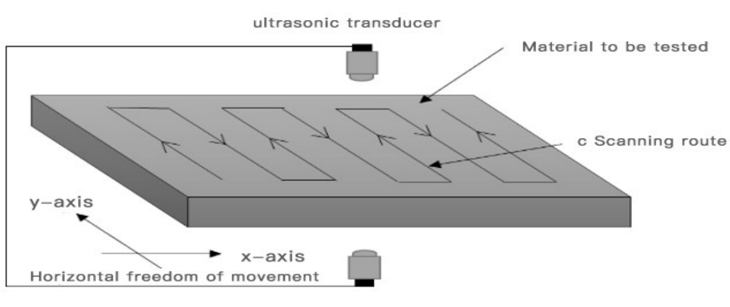

Fig. 2. Ultrasound C-scan

In the ultrasonic A-scan mode, the ultrasonic transmitting transducer and receiving transducer are symmetrically placed on both sides of the plywood. The transmitting transducer is excited by the pulse signal to emit ultrasonic waves. The ultrasonic signals pass through the air and the wood to be tested and are received by the receiving transducer. The air is received by the receiving transducer and is converted into an electrical signal. Then the excitation signal is generated as the starting point, and the ultrasonic signals are received as the end point. The difference of the two times is the ultrasonic flight time. The difference between the two times is the ultrasonic time of flight, and the ultrasonic A-scan delay is analyzed as shown in Fig. 3. The total time of ultrasonic wave propagation from emission to reception at point A is represented as t1+t2+t3, while the propagation time at point B is t1+t3+ta+tb+tc, ultrasonic waves propagate at a consistent speed within the same medium. When ultrasonic waves encounter defects, their propagation speed changes, resulting in different total propagation times. Based on the preceding analysis, ultrasonic time delay can be employed for wood detection. In signal processing correlation analysis, the relationships between variables are categorized into two types: uncertainty and certainty. Non-determinism is represented using correlation theory and statistical probability, typically depicted by a correlation function (Wang 2019).

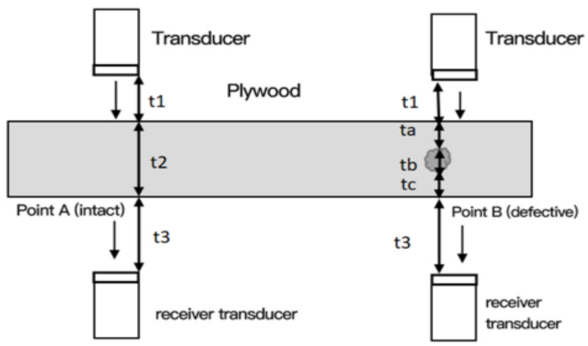

Fig. 3. A-scan delay analysis graph

Let a(t) and b(t) denote two sample functions that undergo stochastic processes {a(t)} and {b(t)}, respectively. The relationship between the value of a(t) at time and the value of b(t) at time ($t+\tau$) is defined as shown in Eq. 1:

$$R_{ab}(\tau) = \lim_{T\to\infty} \frac{1}{T}\int_0^T a\,(t) * b(t+\tau)dt \qquad (1)$$

In Eq. 1, τ represents the delay variable. When a(t) = b(t), then Rxy (τ) the autocorrelation function Rxx (τ):

$$R_{xx}(\tau) = \lim_{T\to\infty} \frac{1}{T}\int_0^T a\,(t) * a(t+\tau)dt \qquad (2)$$

The cross-correlation function of simple harmonic signals can be categorized into functions of signals with different frequency periods and those with the same frequency period (Bai 2017; Guo 2018). If the two simple harmonic signals have the same frequency, Eq. 3 can be derived:

$$R_{xy}(\tau) = \frac{1}{2}X_0Y_0\cos(\omega\tau - \psi) \qquad (3)$$

To enhance measurement accuracy and reduce interference, this study employed the mutual correlation function method for time-delay estimation. Figure 4 presents the A-scan results at points A and B, where the overlapping excitation signals confirm a common propagation starting time, while differences in ultrasonic peak arrival times indicate variations between defective and non-defective positions.

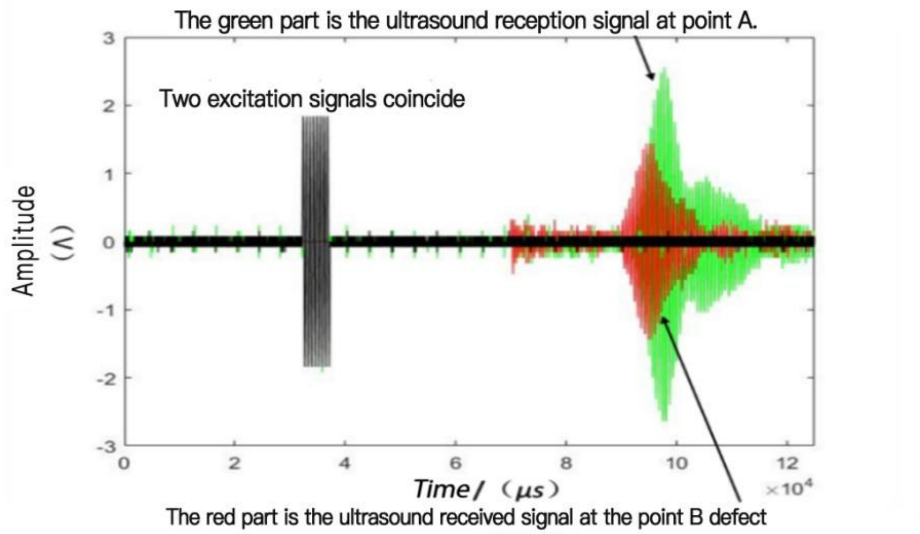

Fig. 4. A and B point scan data waveforms

Hardware Design of Air-coupled Ultrasonic Plywood Inspection System

The hardware design of the plywood air-coupled ultrasonic detection system primarily consists of the ultrasonic C-scanning platform, ultrasonic transmitting module, and ultrasonic signal receiving module. In this study the structural model of the ultrasonic C-scanning platform was constructed, as illustrated in Fig. 5.

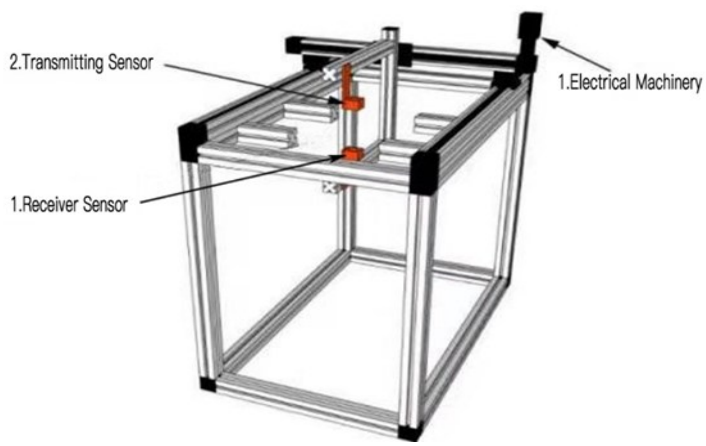

Fig. 5. Platform structure

The platform features a three-dimensional structure, constructed primarily from aluminum alloy. The platform design is primarily divided into three components: the placement plane for the wood to be tested, a circular groove for positioning the ultrasonic probe, and a linear drive scanning mechanism. The platform comprises four short arms made of aluminum alloy, forming the placement plane for the wood to be tested. The upper and lower ends of this plane are vertically aligned to accommodate two round slots, fabricated using plastic 3D printing, which secure the ultrasonic transducers. The distance between the two probes can be adjusted along a straight line using a rectangular slot. The platform utilizes a linear scanning method for the X and Y axes, allowing the ultrasonic transducer to scan along either axis. Scanning is conducted on one axis at a time, which simplifies control and enhances smoothness. The use of a synchronous belt for conduction during scanning contributes to a simple structure with low maintenance costs. The system design incorporates an air-coupled ultrasonic transducer with a focus frequency of 200 kHz, offering advantages in high sensitivity and effective energy directivity.

In the design of the ultrasonic transmitter module, the DAC module of the STM32 is utilized alongside timer TIM to output a voltage value that varies with time. Given that analog signals are continuous while digital signals are discrete (Liu 2004), the use of a DAC to generate a sine wave can only produce points on a sinusoidal curve at specific time intervals. The amplitude of the sine wave excitation signal generated by the DAC module of the STM32 ranges from approximately 0 to 3.3 V. This signal, when applied to the ultrasonic transducer, results in unilateral vibration, generating ultrasonic energy that is only half that produced by bilateral vibration. To enhance the emission energy of the ultrasonic transducer using the same excitation signal, a passive high-pass filter circuit is designed to eliminate the low-frequency DC signal from the microcontroller. The cutoff frequency of this circuit is described by Eq. 4:

$$f = \frac{1}{2*\mathrm{pi}*RC} \quad (4)$$

Due to its high input impedance and low output impedance characteristics, a voltage follower was placed between the microcontroller output and the power amplifier input. This configuration not only provides isolation and buffering but also enhances the circuit's load-carrying capacity. The designed power amplifier circuit features two-stage amplification, utilizing the OPA445 chip along with associated capacitors and resistors for the first amplification stage. This chip is suitable for driving a variety of high-power loads. The second-stage amplifier circuit comprises the OPA544 chip along with relevant capacitors and resistors.

In the design of the ultrasonic transmitted wave signal receiving module, a high-precision amplification circuit is composed of the AD8421 chip along with capacitors and resistors. The ultrasonic transducer generates ultrasonic waves that travel through the air and plywood, resulting in important attenuation by the time they reach the receiving transducer, with amplitudes often only in the millivolt range. To further amplify the ultrasonic signal, the AD8676 chip is employed to design a second-order inverting amplifier circuit. As the ultrasonic wave passes through the pre-processing circuit, second-order inverting amplifier circuit, its signal amplitude can reach the sampling requirements. Thus, in the sampling before the design of the center frequency of 200 kHz AD8676-type active band-pass rate wave circuit, the low-frequency and higher-frequency signals are filtered out.

In the design of the motion control system module, the 57BYGH276 stepping motor was selected. The motor has a holding torque of 1.2 Nm and a basic step angle of 1.8°, providing high accuracy and stability during low-speed operation, which minimizes jitter and instability. The selected driver for the stepper motor is the M542C. The motion control system designed in this study primarily consists of an STM32 main controller, two two-phase four-wire stepper motors, and two stepper motor drivers. The stepper motor driver is divided into a power interface and a control signal interface; the power interface supplies energy to the driver, while the control signal interface of the M542C driver connects to the I/O port of the STM32 microcontroller, which sends control signals to operate the driver.

LabVIEW Visualization of High-speed Data Acquisition and Processing Platform

This platform is a core component of the air-coupled ultrasonic nondestructive testing system for plywood. In accordance with the requirements of the plywood quality inspection system, this study considers factors, such as sampling rate, interface mode, and interface channels, utilizing the LabVIEW (National Instruments, LabVIEW 2020, Austin, TX, USA) development platform for the secondary development of the OSCH02 virtual oscilloscope. Leveraging the high-speed data acquisition capabilities of OSCH02, the platform facilitates the rapid acquisition of ultrasonic transmission signals, inter-correlation processing, and automatic saving of data as a .csv file for imaging. This data can then be analyzed using the plywood host computer software written in Python, ultimately displaying the shape and position of defects in the plywood.

The OSCH02 virtual oscilloscope is controlled through a dynamic link library, specifically named "USBInterFace.dll." This library enables the oscilloscope to perform high-speed acquisition of transmitted waveform data, inter-correlation processing, and data preservation.

In the design of the data acquisition and processing platform, a nested structure using two While loops was implemented, employing functions to achieve the data acquisition objectives. The functions included "USBCtrlTransSimple," "AiReadBulkData," and LabVIEW's built-in "MoveBlock". The corresponding program was developed in accordance with the data acquisition design flow block diagram, as illustrated in Fig. 6.

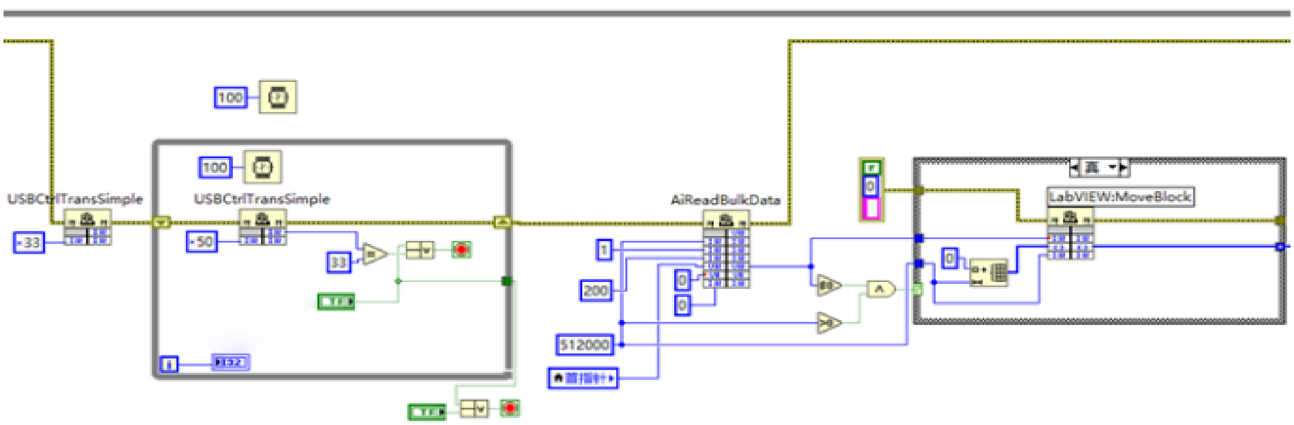

Fig. 6. Data acquisition program

The hardware subsystems described above—the C-scanning platform, the ultrasonic transmitter module, the signal receiving module, and the motion control system—are integrated into a unified plywood quality inspection system. The transmitter module generates a 200 kHz sinusoidal excitation signal that drives the air-coupled transducer; the received signal is amplified and filtered by the receiving module before being passed to the LabVIEW-based data acquisition platform for cross-correlation processing and imaging.

Because the data returned from the data acquisition program was uncorrected and unconverted, it is necessary to perform zero voltage and voltage amplitude calibration. The voltage amplitude calibration data, represented as character data ranging from 0 to 255, was converted to actual voltage values, denoted as "AltitudeByte." To obtain the voltage calibration coefficient from the voltage amplitude calibration data "AltitudeByte," a simple formula was used to convert it into a floating-point coefficient. This coefficient was then applied to calibrate the amplitude in the theoretical formula, as shown in Eq. 5, where "double" represents the floating-point data type:

$$\text{(double) Voltage calibration factor} = \text{(double)}(\text{AltitudeByte} \times 2)/255 \quad (5)$$

The transmitted waveform signal undergoes digital filtering, and the excitation signal is subjected to inter-correlation. Subsequently, the maximum value obtained from the inter-correlation was extracted and saved for defect imaging. Upon completion of the data acquisition process, the data stream containing the voltage values was directed to the automatic data saving program.

System Upper Computer Software Design

In this paper, the upper computer software design of the system is broadly divided into six components: the user interface, C-scan motion control, microcontroller excitation signal output, serial communication, ultrasonic C-scan imaging, and interpolation algorithms. The development of the host computer interface is accomplished using the Python programming language with Qt, specifically PyQt5. Figure 7 illustrates the imaging interface of the host computer, which includes both the pre-interpolation and post-interpolation images. The interface allows users to display images generated from saved data, adjust the interpolation levels along the X and Y axes, select the appropriate interpolation algorithm, generate interpolated images by clicking the interpolation button, and save both the interpolated images and data. Real-time imaging of serial port data is facilitated by the continuous update control on the imaging interface.

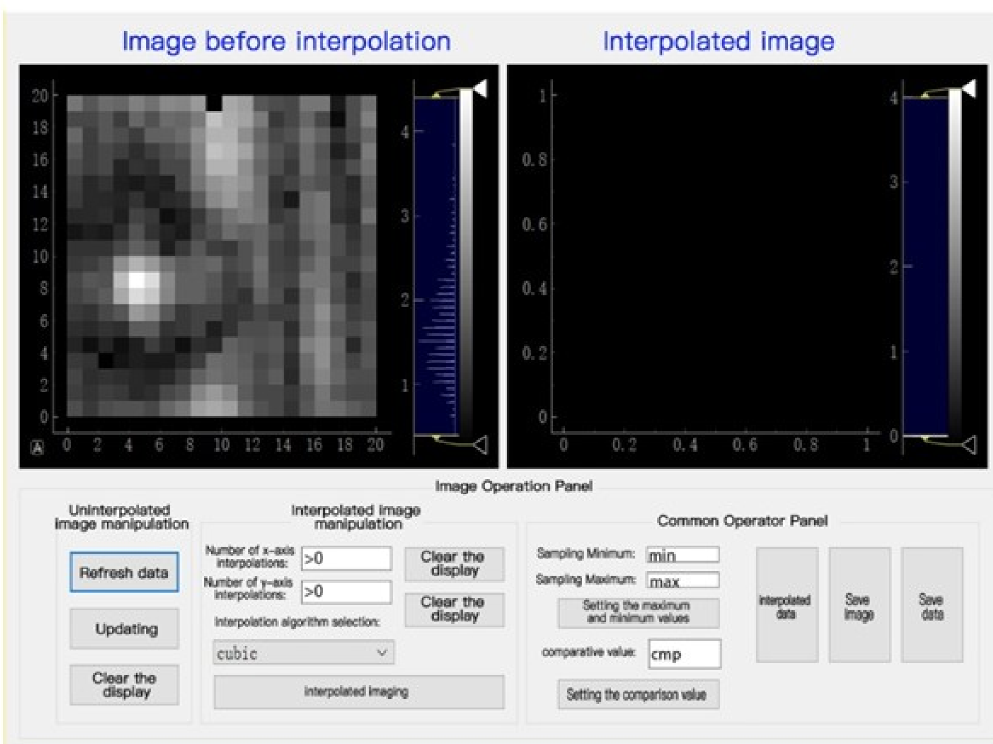

Fig. 7. Data imaging interface

One core component of the system software design is the ultrasonic C-scan motor motion control program, which achieves the predetermined scanning path by controlling the stepper motors along the X and Y axes.

The system uses a DAC to generate a 200 kHz sinusoidal signal for ultrasonic transducer excitation. The signal frequency is calculated as shown in Eq. 6, where T indicates the clock period (1/72000000 s), TIM_Prescaler the prescaler count, TIM_Period the timing period, and N the output points per cycle. Since these are integer values, f cannot exactly equal 200 kHz; with T as 1/72000000, N as 16, TIM_Period as 21, TIM_Prescaler as 0, and the final result of the calculation of f is 204 kHz.

$$f = \frac{1}{T \times (\mathrm{TIM_{Prescaler}}) \times (\mathrm{TIM_{Period}}) \times N} \tag{6}$$

To ensure high accuracy in the detection system designed in this paper, the peak voltage and ultrasonic signal transmission time collected at the scanning sampling points were selected as data for imaging. The imaging results of these two parameters were compared and analyzed to enhance the credibility of the detection outcomes.

In designing the scanning imaging and interpolation algorithm, this system employs the RF sampling method based on actual requirements. The RF method captures the maximum amplitude and transmission time information of the received ultrasonic signals, facilitating imaging based on this data. This imaging method offers advantages such as increased speed, higher efficiency, simpler signal processing, and suitability for online rapid detection.

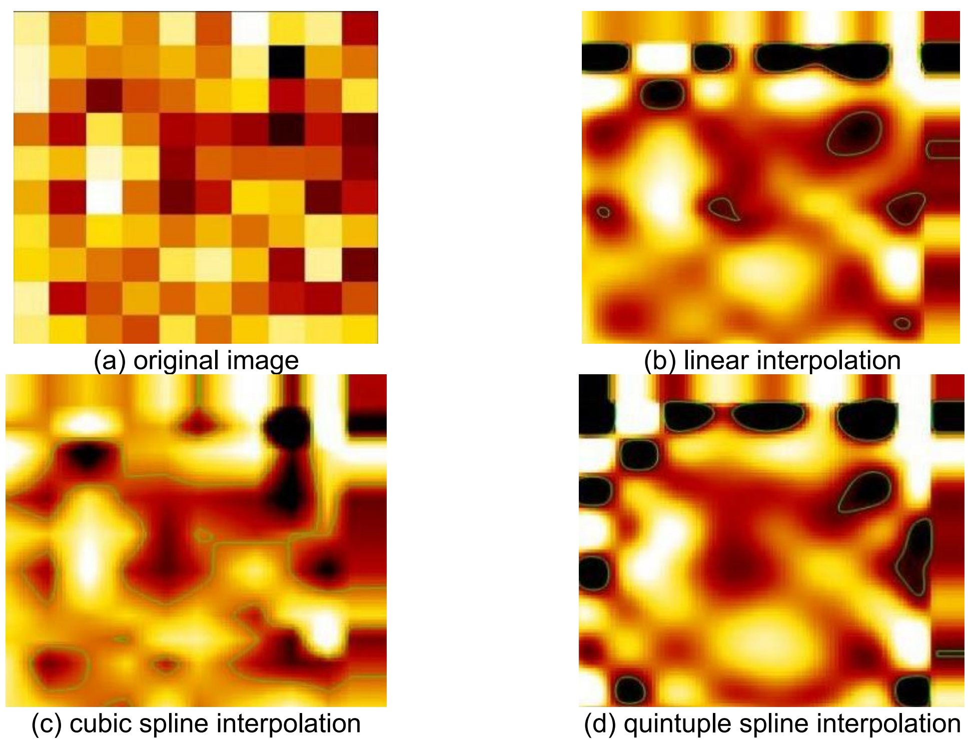

Fig. 8. Spline interpolation with different meshes

To improve imaging quality, spline interpolation is employed. Due to important differences in data collected from neighboring points—often caused by defects—accurate determination of defect locations and shapes can be challenging. The spline interpolation method manages errors *via* multi-order polynomial spline interpolation.

The system employs the interpolate module in the SciPy library to apply three interpolation methods to a given 10 × 10 data set, resulting in an interpolation grid of 100 × 100. The imaging effects of these three interpolation methods are illustrated in Fig. 8.

Analysis of the image results in Fig. 8 reveals that the first-order linear interpolation method exhibits poor imaging quality when the numerical difference between two points is significant, leading to abrupt variations in the resulting image. Additionally, the five-spline interpolation method, due to its excessive number of interpolations, importantly increases computational load, resulting in longer imaging times and distortion in certain areas, which undermines the reliability of the results. In contrast, the third-order spline interpolation method yields superior image quality and reduced processing times. Therefore, this paper adopts the third-order spline interpolation method for interpolating the acquired raw data images.

RESULTS AND DISCUSSION

Plywood Inspection System Testing

Ultrasonic waves penetrating the plywood are received by the opposite ultrasonic transducer, initially processed through the receiver module circuit, and subsequently acquired and processed by the LabVIEW-based high-speed data acquisition and processing platform. This platform captures the excitation signals, received signals, and performs cross-correlation processing of the signal waveforms, as illustrated in Fig. 9. According to the propagation characteristics of ultrasonic waves, a majority of the sound waves are reflected when encountering obstacles, with only a small portion transmitting through. Consequently, if the distance between the ultrasonic transducer and the material being tested is not optimal, the emitted energy may cancel with the reflected energy, resulting in significant attenuation. Moreover, the suitable distance varies depending on the material.

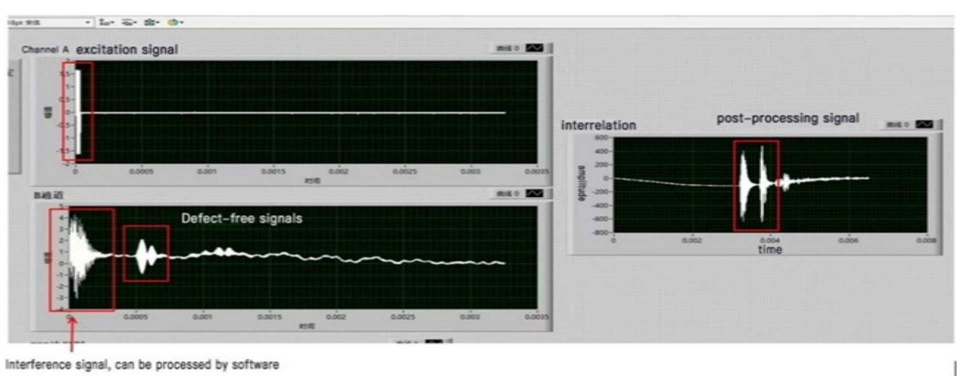

Fig. 9. Ultrasonic excitation signal, received signal, and cross-correlation processing signal

In this study, different distances were experimentally validated, with vertical distances of the two ultrasonic transducers set at 10 cm, 15 cm, 20 cm, and 25 cm, respectively. The results of these experiments are depicted in Fig. 10. From the data presented in Figs. 9 and 10, it is evident that the best received signal occurred when the vertical distance between the ultrasonic transducers was 15 cm. Although the amplitude of the received signal was larger at a distance of 10 cm, it risks signal overlap. In contrast, at distances of 20 cm and 25 cm, the amplitude of the received signal decreased importantly. Therefore, the optimal distance between the two ultrasonic transducers in this plywood quality inspection system was determined to be 15 cm. Given that the plywood specimen has a thickness of 10 mm and the two transducers are symmetrically placed on both sides, the distance from each transducer face to the nearest plywood surface is approximately 7 cm.

Each measurement point receives only 8 pulses of 200 kHz excitation with very low acoustic energy; consequently, any air temperature rise is negligible and does not affect the amplitude or time-delay imaging results.

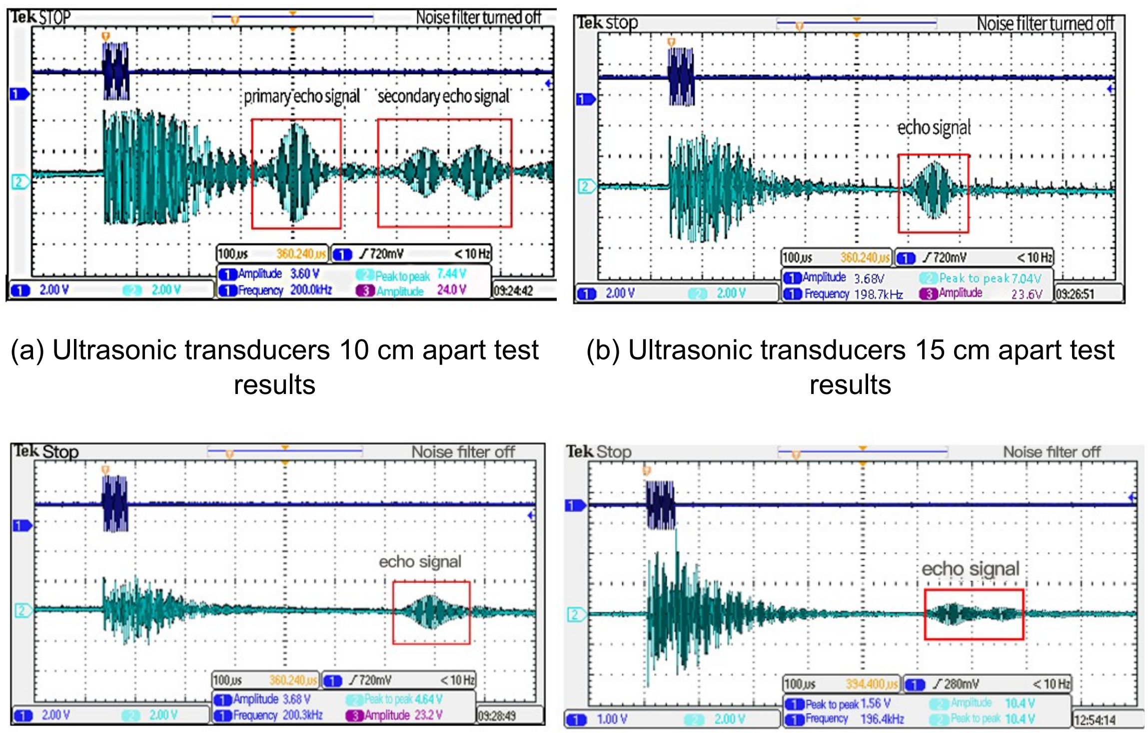

(a) Ultrasonic transducers 10 cm apart test results

(b) Ultrasonic transducers 15 cm apart test results

(c) Ultrasonic transducers 20 cm apart test results

(d) Ultrasonic transducers 25 cm apart test results

Fig. 10. Graph of detection results at different distances

Detection System Scanning Parameter Selection

To improve the detection speed of the C-scan and minimize control errors, the plywood quality inspection system required a thorough evaluation. First, the single-axis accuracy of the scanning process was determined based on the size of each sampling point within the plywood divisions. The basic step angle of the stepper motor is 1.8°, and with a driver selecting 10 subdivisions, each trigger pulse allowed the stepper motor to rotate 0.18°. The total number of selected subdivisions was 25,600.

Figure 11 presents a test sample with an interpolation number of 500, which was scanned and imaged using scanning step lengths of 3 mm, 2 mm, and 1 mm, respectively. The scanning results corresponding to a step length of 2 mm are illustrated in Fig. 12. In Fig. 12, the black and dark areas represent low-value regions, while the white areas denote high-value regions, and the yellow areas indicate even higher values.

Fig. 11. Test plywood

The specific scanning results are shown in Fig. 12.

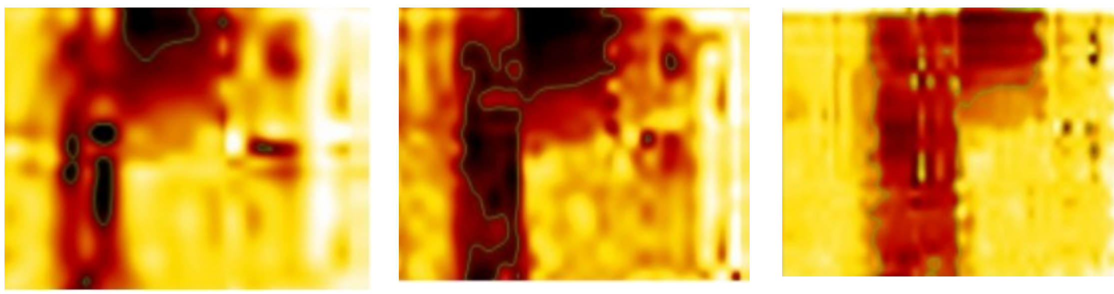

(a) 3 mm scanning imaging (b) 2 mm scanning imaging (c) 1 mm scanning imaging

Fig. 12. Scanning results with different scanning steps

As the scanning step size increased, the resolution of the imaging tended to decrease. However, at a scanning step size of 1 mm, despite achieving high resolution, the image quality importantly declined, adversely affecting the localization of defect detection. Consequently, the experiments conducted in this paper adopted a scanning speed of 20 mm/s and a step length of 2 mm as the optimal scanning parameters.

Effect of Interpolation Number on Imaging Results

Different interpolation numbers importantly affect the smoothness of imaging. As illustrated in Fig. 13, an increase in the number of interpolations resulted in a smoother and improved image quality. However, an excessively high interpolation count can lead to increased computational demands and a reduction in imaging speed. Therefore, this paper selected a 500 × 500 interpolation number for subsequent imaging tests.

Analysis of Imaging Results for Plywood Defect Detection

In the parameter determination of the plywood quality inspection system, the parameters were set as follows: the excitation waveform was sinusoidal, the pulse frequency was 200 kHz, the scanning speed was 20 mm/s, the scanning step was 2 mm, the number of scanning points was 25 × 25, and the number of imaging interpolations was 500 × 500. To validate the accuracy and feasibility of the plywood quality inspection system designed in this paper, the authors selected a plywood specimen measuring 500 mm × 300 mm × 10 mm, with an average density of 0.65 g/cm^3 and an average moisture content of 26%. The system was used to detect various defects in the plywood, including bulging, gluing, seam separation, knots, and wormholes.

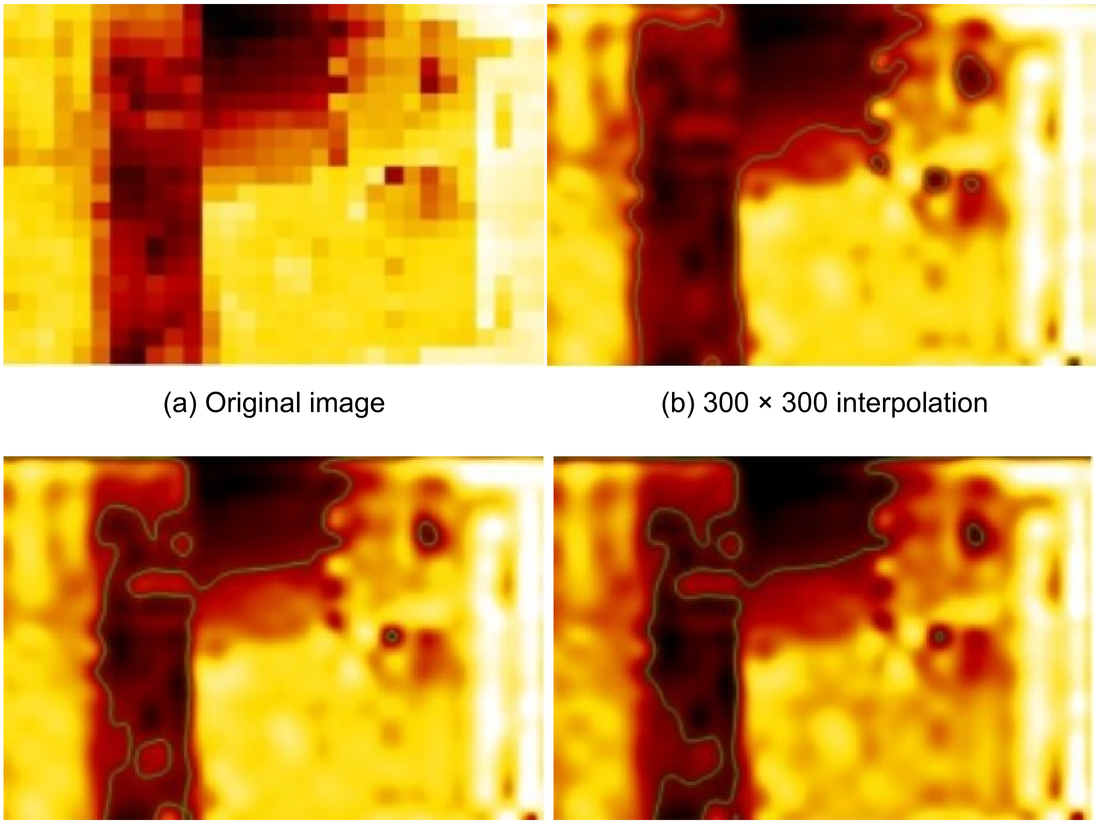

(a) Original image (b) 300 × 300 interpolation

(c) 500 × 500 interpolation (d) 1000 × 1000 interpolation

Fig. 13. Display effect of images with different interpolation number

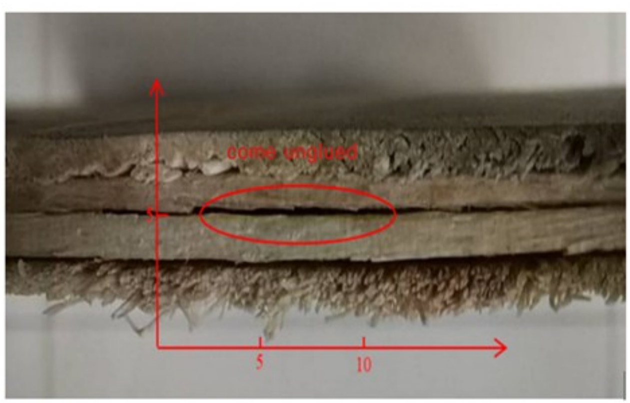

Fig. 14. Cross-section of gluing defects

Due to the challenges in recognizing defects, such as blistering and open gluing through visual inspection, the authors collaborated with a local plywood production factory to prepare a specimen containing both blistering and open gluing defects, measuring 500 mm × 300 mm × 10 mm. The open glue defects are illustrated in Fig. 14, which depicts a cross-section of the plywood after sawing. The signals at the plywood without and with defects are shown in Fig. 15.

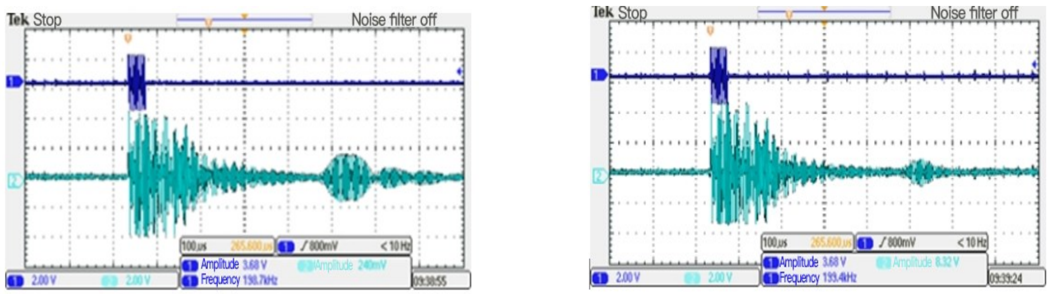

(a) Defect-free signals (b) Defective signals

Fig. 15. Plywood scanning results

In both the intact regions and the exterior of the plywood, the attenuation of ultrasonic waves during penetration is minimal, resulting in relatively high signal amplitudes in the absence of defects. Conversely, in regions with bulging or gluing defects, the signal energy experiences greater attenuation, resulting in lower amplitudes of the received ultrasonic signals. The varying amplitudes of the ultrasonic signals collected from different areas validate the feasibility of this non-destructive testing (NDT) system. Upon sawing through the locations identified with open glue defects, the imaging results were largely consistent with the actual defects. Thus, this system can accurately detect the quality of open glue and bulging defects.

For the knots quality inspection of plywood, a specimen containing knots, as shown in Fig. 16, was selected for testing, measuring 500 mm × 200 mm × 10 mm, with the knot defect measuring 14 mm × 15 mm.

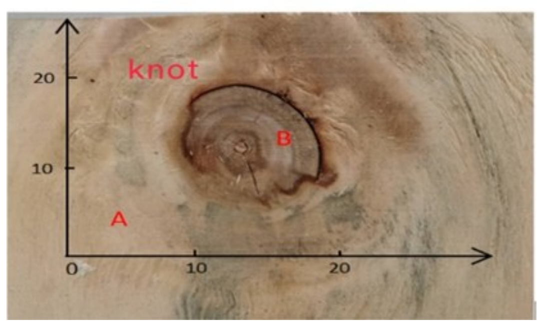

Fig. 16. Nodal defect diagram

Prior to C-scan imaging, the movement of the ultrasonic transducer was controlled to points A and B for ultrasonic A-scan. The detection signals at these two points were analyzed, and the signal amplification gain was adjusted based on the amplitude of the detection signal to avoid data anomalies caused by excessive gain. After several trials, a gain of 63 dB was selected for the C-scan imaging of the knot defects in the plywood. Figure 17 presents the detection signals at points A and B.

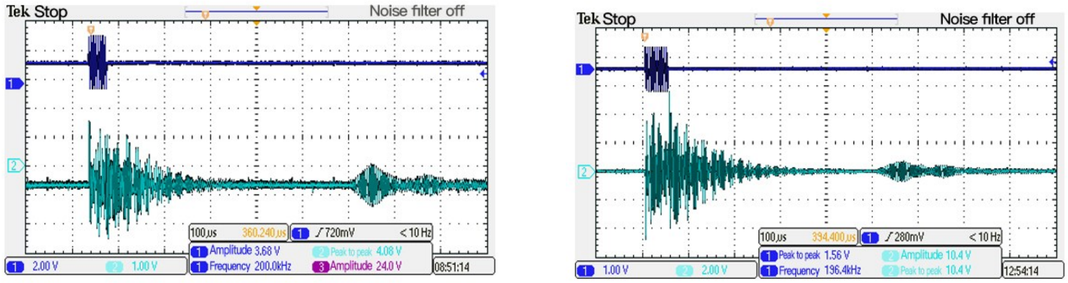

(a) Signal detected at A (b) Signal detected at B

Fig. 17. Detection signal

The higher density of knots at point B caused significant signal attenuation. According to Fig. 17, the C-scan imaging shows reddish dark coloration at the knot (small amplitude), while other regions appear greenish yellow (larger amplitudes), consistent with theoretical analysis and allowing intuitive visualization of the knot's shape.

The ultrasonic C-scan imaging image of the nodule is shown in Fig. 18.

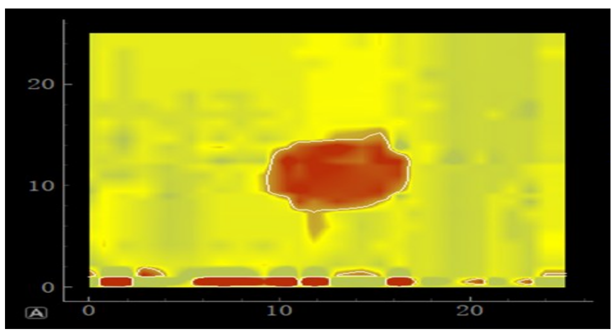

Fig. 18. Nodal imaging diagram

Wormholes are tunnel-like cavities (typically 1 to 5 mm in diameter) created by wood-boring insects prior to or during plywood manufacturing, appearing as irregular circular or elliptical voids in cross-section. They may exist on the core veneer surface or entirely within the interior layers, both compromising structural integrity. A specimen containing wormholes, as depicted in Fig. 19, was also selected for testing, measuring 550 mm × 200 mm × 10 mm, with wormhole sizes of 10 mm × 20 mm.

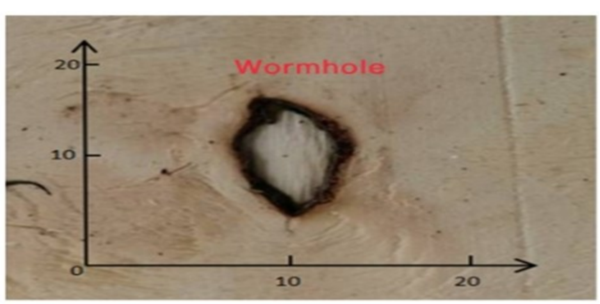

Fig. 19. Diagram of wormhole defects

The ultrasonic C-scan imaging results of the wormholes are shown in Fig. 20. The color at the wormhole appears reddish dark, with a small amplitude, while surrounding areas predominantly exhibit yellowish white coloration with larger amplitudes. This observation is consistent with theoretical analysis results and effectively illustrates the shape of the wormholes.

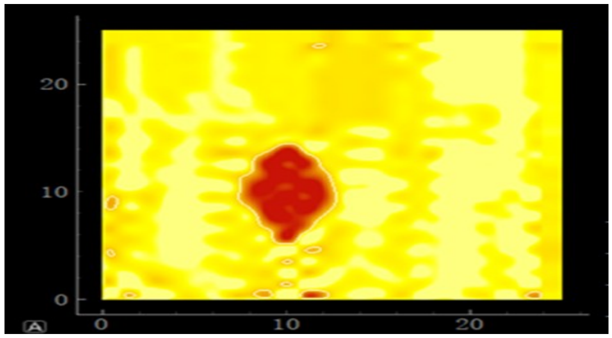

Fig. 20. Scanning imaging of wormhole C

Notably, the wormhole detection experiment also included specimens where the defect existed entirely within the interior core veneer, invisible from both surfaces. The C-scan imaging successfully identified the internal void and portrayed its approximate X-Y dimensions, confirming the system's ability to detect invisible defects. Future work will incorporate artificially created rectangular voids of known dimensions for further quantification.

CONCLUSIONS

1. This paper has presented the design of a plywood quality inspection system based on air-coupled ultrasound, which encompasses both hardware and software design, as well as verification through plywood inspection tests.
2. The hardware design primarily includes the construction of the ultrasonic C-scan platform, selection of core detection devices, development of the signal excitation and processing modules, and the design of the motion control module.
3. The software design focuses on the development of the host computer interface, C-scan motion control, MCU excitation signal output, serial communication, ultrasonic C-scan imaging, and interpolation algorithms.
4. Testing and validation experiments demonstrated that the system effectively detected common plywood defects, such as blisters and seams, with accurate positioning, allowing for the determination of defect location and shape. This capability provides essential technical support for the online quality inspection of plywood products.
5. With the adopted scanning parameters (20 mm/s, 2 mm step, 25 × 25 points), the C-scan observation time is approximately 62.5 seconds per specimen area, with subsequent computation completed within 10 to 15 seconds, yielding a total inspection time of less than 80 seconds. Multiple transducer arrays could further reduce this time for production-line applications.

ACKNOWLEDGMENTS

The 2024 Forestry Science and Technology Innovation and Extension Project in Jiangsu Province (LYKJ[2024]05).

REFERENCES CITED

Akseli, I., Dey, D., and Cetinkaya, C. (2010). "Mechanical property characterization of bilayered tablets using nondestructive air-coupled acoustics," *AAPS PharmSciTech* 11(1), 1210-1219. https://doi.org/10.1208/s12249-009-9352-9

Bai, Z. (2017). *Design and Research of High-speed Dynamic Balancing Test System for Flexible Rotor,* Master's Thesis, Shenyang University of Science and Technology, Shenyang, China.

Bustamante, L., Jeyaprakash, N., and Yang, C. (2020). "Evaluation of defect detection in aluminium, CFRP and epoxy resin plates using non-contact air-coupled ultrasonic waves," *International Journal of Precision Engineering and Manufacturing* 21(10), 1843-1856.

Castaings, M., Cawley, P., Farlow, R., and Hayward, G. (1998). "Single sided inspection of composite materials using air coupled ultrasound," *Journal of Nondestructive Evaluation* 17(1), 12-19.

Gui, Q., Jin, C. E., and Zhou, J. P. (2016). "Application of air-coupled ultrasound technology in nondestructive testing of aerospace composites," *Nondestructive Testing* 38(08), 6-11. https://doi.org/10.11973/wsjc201608002

Guo, J. C. (2018). *Research and Design of Transmitting Circuit of Underground Pipe Detection System*, Master's Thesis, Shandong University of Science and Technology, Qingdao, China. https://doi.org/10.27275/d.cnki.gsdku.2018.000322

In, C.-W., Schempp, F., Kim, J.-Y., and Jacobs, L. J. (2015). "A fully non-contact, air-coupled ultrasonic measurement of surface breaking cracks in concrete," *Journal of Nondestructive Evaluation* 34, 272. https://doi.org/10.1007/s10921-014-0272-6

Khan, N., Pu, C., Li, X., He, Y. L., Zhang, L., and Jing, C. (2017). "Permeability recovery of damaged water sensitive core using ultrasonic waves," *Ultrasonics Sonochemistry* 38, 381-389. https://doi.org/10.1016/j.ultsonch.2017.03.034

Li, H., and Zhou, Z. (2019). "Detection and characterization of debonding defects in aeronautical honeycomb sandwich composites using noncontact aircoupled ultrasonic testing technique," *Applied Sciences* 9(2), 283. https://doi.org/10.3390/app9020283

Li, J., Cao, L., and Wang, D. F., and Fu, C. (2020). "Radar time-frequency signal inter-correlation speed measurement algorithm based on wavelet noise reduction," *Modern Electronic Technology* 43(9), 14-20. https://doi.org/10.16652/j.issn.1004-373x.2020.09.004

Li, S. (2020). *Research on the Theory and Application of Location Sensing of Intelligent Devices Based on Ultrasound,* Master's Thesis, Nanjing University of Aeronautics and Astronautics, Nanjing, China. https://doi.org/10.27239/d.cnki.gnhhu.2020.001378

Liang, X., Cai, C. H., He, Y. H., and Wang, Z. (2022). "Design and development of composite plywood integrating fireproof, waterproof and abrasion resistance," *Forest Industry* 59(11), 1-6. https://doi.org/10.19531/j.issn1001-5299.202211001
Liu, A. (2019). *Research on Plate Structure Inspection Technology Based on Non-contact Air-coupled Ultrasound*, Ph.D. Dissertation, Dalian University of Technology, Dalian, China.
Liu, L. Q. (2004). "Analysis and research on the application of correlation analysis technology in engineering measurement," *Journal of Shenyang Institute of Aeronautics and Astronautics* 5, 67-69. https://doi.org/10.3969/j.issn.2095-1248.2004.05.025
Livings, R., Dayal, V., and Barnard, D. (2016). "Damage detection in a multi-layered, multi-material composite using air-coupled ultrasonic resonance imaging," *Journal of Nondestructive Evaluation* 35, 55. https://doi.org/10.1007/s10921-016-0368-2
Quattrocchi, A., Freni, F., and Montanini, R. (2020). "Air-coupled ultrasonic testing to estimate internal defects in composite panels used for boats and luxury yachts," *International Journal on Interactive Design and Manufacturing (IJIDeM)* 14(01), 35-41. https://doi.org/10.1007/s12008-019-00611-5
Sanabria, S. J., Mueller, C., Neuenschwander, J., Niemz, P., and Sennhauser, U. (2011). "Air-coupled ultrasound as an accurate and reproducible method for bonding assessment of glued timber," *Wood Science and Technology* 45(4), 645-659. https://doi.org/10.1007/s00226-010-0357-z
Shi, R. (1989). "Ultrasonic detection of surface opening crack depth," *Journal of Qiqihar Teachers College (Natural Science Edition)* 02, 29-34.
Song, Y. B., Ma, X. S., Tao, Y. H., Sa, P.C., and Li, P. X. (2020). "Research and realization of ultrasonic anti-recording shielding based on acoustic parametric array theory," *Journal of Beijing Institute of Technology* 40(12), 1282-1288. https://doi.org/10.15918/j.tbit1001-0645.2019.252
Wang, K. (2019). *Analysis of Temperature Force and Vibration State Detection of Rails in High-speed Railroad*, Ph.D. Dissertation, Dalian University of Technology, Dalian, China.
Wang, Y. (2022). "Research on financial support for forestry technology innovation based on gray correlation analysis," *China Forestry Economy* 05, 39-43. https://doi.org/10.13691/j.cnki.cn23-1539/f.2022.05.007
Wang, Z. H., Gao, Z. Z., Wang, Y. L., Cao, Y., Wang, G. G., Liu, B., and Wang, Z. (2015). "A new dynamic testing method for elastic, shear modulus and Poisson 's ratio of concrete," *Construction and Building Materials* 100, 129-135. https://doi.org/10.1016/j.conbuildmat.2015.09.060
Wang, Z. H., Wang, Y. L., Cao, Y., and Wang, Z. (2016). "Measurement of shear modulus of materials based on the torsional mode of cantilever plate," *Construction and Building Materials* 124, 1059-1071. https://doi.org/10.1016/j.conbuildmat.2016.08.104
Wang, Z., Xie, W., Wang, Z., and Cao, Y. (2018). "Strain method for synchronous dynamic measurement of elastic, shear modulus and Poisson's ratio of wood and wood composites," *Construction and Building Materials* 182, 608-619. https://doi.org/10.1016/j.conbuildmat.2018.06.139

Zhang, D., Pan, Y. D., Li, L. B., and Zhao, J. F. (2016). "Unilateral non-contact ultrasonic nondestructive testing method for plate back defects," *Experimental Mechanics* 31(04), 525-533. https://doi.org/10.7520/1001-4888-16-001

Article submitted: January 27, 2025; Peer review completed: April 5, 2026; Revised version received: June 2, 2026; Further revised version received: June 10, 2026; Accepted: June 11, 2026; Published: June 29, 2026.
DOI: 10.15376/biores.21.3.7572-7591